Buoyant displacement flow of immiscible fluids in inclined ducts: A theoretical approach

A. Hasnain[1] and K. Alba[2,a)]
[1]*Department of Mechanical Engineering, University of Houston, N207 Engineering Building 1, Houston, Texas 77204, USA*
[2]*Department of Engineering Technology, University of Houston, 304 Technology Building 2, Houston, Texas 77204, USA*

(Received 1 December 2016; accepted 19 April 2017; published online 5 May 2017)

We study the buoyant displacement flow of two immiscible Newtonian fluids in an inclined duct (two-dimensional channel) theoretically. The fluids may have different viscosities. The displacing fluid is denser than the displaced one, i.e., a density-unstable configuration. For simplicity, the fluids are assumed to behave as neutrally wetting in the vicinity of duct walls. The small diameter-to-length ratio of the duct considered ($\delta \ll 1$) has been used as the perturbation parameter in developing a *lubrication* model (negligible inertia). Appropriate *Navier-slip* conditions have been applied at the walls to overcome contact-line problem singularity. The lubrication model developed has then been numerically solved using a robust total variation diminishing finite difference scheme. Completely different flow patterns have been observed compared to the miscible limit. Fluids immiscibility is found to cause a *capillary ridge* in the vicinity of the displacing front, which diminishes as the surface tension is increased. For small values of surface tension parameter, the fluids immiscibility is found to decelerate the advancement of interpenetrating heavy and light layers. More efficient displacement (less fingering within the displacing layer) has been observed at small density differences and when the displacing fluid is more viscous than the displaced one. The limit of zero imposed velocity corresponding to the *exchange* flow has further been considered in the lubrication model. An interesting jump in the interface height occurs close to the vicinity of the gate region due to the immiscibility, which has been similarly reported in other recent computational works. Detailed mathematical notes on the similarity solution of the flow at long times are moreover provided. Investigating the short-time dynamics of the flow reveals the dominance of diffusive surface tension effects over buoyancy. *Published by AIP Publishing.* [http://dx.doi.org/10.1063/1.4982896]

I. INTRODUCTION

Removal or displacement flow of one fluid by another is widely observed in nature. These flows also have many applications such as in the petroleum industry, coating and co-extrusion, Gas Assisted Injection Molding (GAIM), biomedical contexts (mucus, biofilms), cleaning of equipment, food processing, and personal care.[1–11] Much of the motivation for the current study comes from common multi-fluid flow operations present in the construction and completion of oil and gas wells, e.g., primary cementing, drilling, and hydraulic fracturing. Geothermal, CO_2 sequestration and domestic water distribution wells are cemented using the very same techniques as in the oil and gas industry. Throughout the primary cementing process, a series of fluids are pumped down the casing, which can be tilted at any angle varying from horizontal to vertical, to remove the drilling mud and/or other *in situ* fluids.[1] Operational failures can become highly expensive and catastrophic as seen recently in the Gulf of Mexico. For conventional resources, a Water-Based Mud (WBM) is often used during drilling, which is *miscible* with cement slurry. For rapidly developing unconventional resources, the use of a miscible WBM can nonetheless cause several problems associated with swelling shales and differential sticking. These problems can be resolved by changing from a WBM to an *immiscible* Oil-Based Mud (OBM) shown to improve the cement bond and thus zonal isolation.[12] While the displacement flow of miscible fluids has been explored in depth in the literature experimentally, computationally, and analytically by Refs. 13–28, our knowledge of immiscible fluids mixing is very limited, due to the increased complexity arising from the presence of fluids interfacial tension as well as their wetting/non-wetting characteristics when in contact with a solid geometry. Currently there exist only a few experimental[29] and computational[30,31] works on buoyant immiscible displacement flows demanding further research in this area.

It has been observed that depending on the inclination angles and other flow parameters, various *viscous*, *transitionary*, and *diffusive* displacement flows may emerge characterized by the degree of fluids interfacial instability.[19] Viscous flows are generally observed for close-to-horizontal inclination angles.[23] As the duct is inclined toward vertical, the interfacial instabilities grow causing transitionary and diffusive flows. The fluid-fluid displacement in confined geometry even in the viscous regime is indeed a complicated problem.

a)Author to whom correspondence should be addressed. Electronic mail: kalba@uh.edu

Computational approaches to study such flows always have limitations. On the other hand, *thin-film lubrication-style* models are proven to be amongst the most robust analyses present. The evolution of these models in the literature for miscible fluids has been such that first simple two-dimensional cases are introduced,[26] and then complex three-dimensional effects of channels[32,33] and pipes[18,23] are considered. Despite the geometrical difference, many underlying physics of computationally cheap two-dimensional problem is still similar to that of a three-dimensional duct emphasizing the effectiveness of the former. In line with the advancement of lubrication style studies for a miscible case, we aim to introduce, for the first time, an immiscible two-dimensional model paving the way for more complex experimental and theoretical analyses to come in the future.

The lubrication model is first derived in Section II. The Total Variation Diminishing (TVD) finite difference scheme used in numerically solving the derived model is explained in Section III. In the presentation of our results in Section IV, we will first discuss the case of *displacement* flows and then consider *exchange* flows as a limiting case (zero imposed flow). The paper closes with a brief summary in Section V.

II. LUBRICATION MODEL DERIVATION

We aim to construct a lubrication model in a simplified near-horizontal 2D channel geometry shown schematically in Fig. 1. The heavy fluid with density $\hat{\rho}_H$ and viscosity $\hat{\mu}_H$ displaces the light one with $\hat{\rho}_L$ and $\hat{\mu}_L$ in a channel with thickness $\hat{D}$, inclined at an angle β measured from vertical. The mean imposed velocity is $\hat{V}_0$. The lubrication model governing the viscous displacement of two *miscible* generalized Newtonian fluids has been developed in the work of Taghavi *et al.*[26] It is not difficult to show that for the immiscible flow shown in Fig. 1, the governing streamwise and depthwise momentum equations in the heavy layer reduce to

$$0 = -p_x + \frac{1}{1-\phi}\chi + u_{yy}, \tag{1}$$

$$0 = -p_y - \frac{1}{1-\phi}, \tag{2}$$

where $\chi = 2Re\cos\beta/Fr^2$ is the driving buoyancy component as a measure of the relative importance of the slope of the channel to the slope of the interface, and $\phi = \hat{\rho}_L/\hat{\rho}_H$. Here,

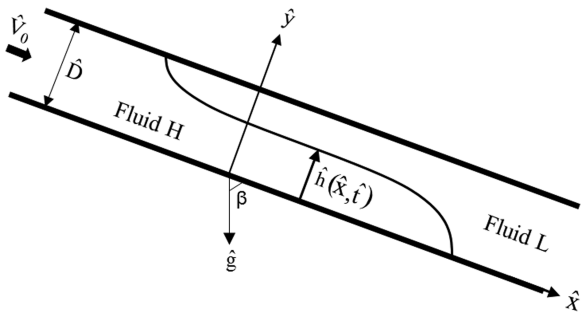

FIG. 1. Schematic of the immiscible displacement flow used in the lubrication model analysis. Note that dimensional notations are used in the figure. The interface shape is illustrative only.

$Re = \hat{V}_0\hat{D}/\hat{\nu}$ is the Reynolds number, with $\hat{\nu}$ being the kinematic viscosity defined using the mean density $\hat{\rho} = (\hat{\rho}_L + \hat{\rho}_H)/2$ and the viscosity of the heavy fluid, $\hat{\mu}_H$. Moreover, $Fr = \hat{V}_0/\sqrt{At\hat{g}\hat{D}}$ is the Froude number with $At = (\hat{\rho}_H - \hat{\rho}_L)/(\hat{\rho}_H + \hat{\rho}_L)$ and $\hat{g}$ being the Atwood number and gravitational acceleration, respectively. We have scaled the streamwise and depthwise distances by $\hat{D}/\delta$ and $\hat{D}$, respectively, where $\delta = \hat{D}/\hat{L}$ is the channel aspect ratio industrially taken to be very small ($\delta \ll 1$).[1] The pressure has been scaled by $\hat{\mu}_H\hat{V}_0/\delta\hat{D}$. Similarly, for the light fluid layer we can have

$$0 = -p_x + \frac{\phi}{1-\phi}\chi + mu_{yy}, \tag{3}$$

$$0 = -p_y - \frac{\phi}{1-\phi}, \tag{4}$$

where $m = \hat{\mu}_L/\hat{\mu}_H$ is fluids viscosity ratio. Integrating (2) within the heavy fluid layer ($0 < y < h$) gives

$$p = p_0(x,t) + \frac{1}{1-\phi}(\chi x - y), \qquad 0 \le y \le h, \tag{5}$$

where we have defined $p_0(x, t)$ as

$$p_0(x,t) = p(x,0,t) - \frac{\chi}{1-\phi}x. \tag{6}$$

Integrating (4) in the depthwise direction gives the pressure field within the light fluid layer as

$$p = p_0(x,t) + \frac{1}{1-\phi}(\chi x - \phi y) - h + Wh_{xx}, \qquad h \le y \le 1, \tag{7}$$

where $W = \hat{\sigma}\delta^2/(\hat{g}\hat{D}^2(\hat{\rho}_H - \hat{\rho}_L)\sin\beta)$ is the Laplace number with $\hat{\sigma}$ being the interfacial tension between the two fluids. Note that the last term in (7) is the jump in pressure due to the capillary force. In order to capture surface tension effects we have assumed $W \backsim O(1)$.

The pressure expressions (5) and (7) can now be used in the streamwise momentum equations (1) and (3) to give

$$0 = -p_{0,x} + u_{yy}, \qquad 0 \le y \le h, \tag{8}$$

$$0 = -p_{0,x} + mu_{yy} - \chi + h_x - Wh_{xxx}, \qquad h \le y \le 1. \tag{9}$$

Using the appropriate boundary and interfacial conditions, Equations (8) and (9) can be integrated with respect to y to give the streamwise velocity closures in each layer. In the case of miscible fluids, the standard no-slip condition at the lower ($y = 0$) and upper ($y = 1$) walls may be used as well as the velocity and shear stress homogeneity conditions at the interface ($y = h$) to solve for the velocity field.[26] However, in the case of immiscible fluids, one faces the well-known *contact-line* problem due to the singularity of the stress at the walls. Many authors have worked intensely for decades to address this issue suggesting a wide range of remedies. The simplest solution is to assume a narrow *precursor* film in the vicinity of the wall, which works well for completely wetting fluids, i.e., very small contact angles.[34,35] Others have proposed models based on *Navier-slip* conditions.[34,36–38] For simplicity and assuming two *neutrally wetting* fluids, we apply Navier-slip conditions at the lower and upper walls exactly as proposed by[34,36]

$$u = \frac{\alpha}{3h}u_y \qquad at\ y = 0, \tag{10}$$

$$u = \frac{\alpha m}{3(h-1)} u_y \quad at\ y = 1. \tag{11}$$

Here, α is a small slip parameter chosen to be 0.001 in our study. Note that h and $h - 1$ appear in the denominator of (10) and (11), respectively, to ensure enhancement of the slip velocity when approaching the walls ($h \to 0$ and 1). Spaid and Homsy[34] showed that in the context of contact line flows, there is a negligible dependency of the results on the slip parameter as long as α is chosen to be small. The homogeneity of the velocity and stress at the interface requires

$$[u] = 0, \left[\tau_{xy}\right] = 0 \quad at\ y = h, \tag{12}$$

where [] denotes the jump of the given quantity. Note that $\tau_{xy} = u_y, mu_y$ for the heavy and light fluids, respectively. The last condition needed to solve systems (8) and (9) for the velocity closures is the total flow constraint

$$\int_0^1 u dy = 1. \tag{13}$$

The velocity in heavy and light layers can then be obtained as

$$u = p_{0,x} y^2/2 + c_1 y + c_2, \quad 0 \le y \le h, \tag{14}$$

$$u = (p_{0,x} + \chi - h_x + W h_{xxx}) y^2/(2m) + d_1 y + d_2, \quad h \le y \le 1, \tag{15}$$

where $p_{0,x}, c_1, c_2, d_1$, and d_2 are coefficients given in Appendix A. The lower layer flow rate flux function, q, can eventually be calculated as

$$q = \int_0^h u dy, \tag{16}$$

which is found to be in the form of

$$q = q_A + (\chi - h_x + W h_{xxx}) q_B. \tag{17}$$

Here, q_A and q_B, which are given in Appendix B as functions of h, m, and α, represent the advective and buoyancy-driven components of the flux function, q, respectively.[26] In order to gain a better understanding of the behavior of the flux function, q, its variation as well as that of its derivative, q_h (required in Sections III and IV), is plotted versus h in Figs. 2(a) and 2(b), respectively, for various χ values. For simplicity, we have, moreover, set $h_x = h_{xxx} = 0$, $m = 1$. It can be seen that $q \to 0, 1$ as $h \to 0, 1$. For low values of χ, the lower layer flow rate, q, remains bounded between [0, 1] (Fig. 2(a)). However, as χ is increased (enhanced counter-current) q may exceed 1 to conserve mass across the channel. The derivative of q, i.e., q_h shows a less monotonic dependency on h (Fig. 2(b)). The variation of q_h amplitude is enhanced with χ. The more interesting observation is rather a sharp change of q_h close to the channel walls $h = 0$, 1. In all the cases shown, $q_h \to 1.5$ as $h \to 0, 1$ as indicated in the inset of Fig. 2(b). This is purely due to the implementation of the wall-slip conditions (10) and (11) in our lubrication model to overcome contact line singularity. Note that in the case of miscible fluids $q_h \to 0$ as $h \to 0, 1$.[26]

Finally, the kinematic condition at the interface reads

$$h_t + q_x = 0. \tag{18}$$

Note that in (18), the time is naturally scaled by $\hat{D}/(\delta \hat{V}_0)$. Plugging the flux function (17) into (18) gives

$$h_t + F_x(h) + Q_x(h, h_x) + R_x(h, h_{xxx}) = 0, \tag{19}$$

where

$$F(h) = q_A + \chi q_B, \tag{20}$$

$$Q(h, h_x) = -h_x q_B, \tag{21}$$

$$R(h, h_{xxx}) = W q_B h_{xxx}. \tag{22}$$

III. NUMERICAL SCHEME

Equation (19) contains advection as well as second and fourth order diffusion terms and should be treated with extreme care from a numerical perspective. Our methodology to solve (19) in space, x, and time, t, is based on a total variation diminishing (TVD) finite difference scheme that combines the robust explicit high-resolution scheme of Ref. 39 for the advection term with an explicit-implicit scheme similar to that of Ref. 40 for diffusion terms. Note that one cannot practically use a fully explicit scheme for the entire terms in (19) because the required stable time step would then be on the order of $dt \sim O(dx^4)$ due to the presence of the fourth-order diffusion term.[41] Discretizing (19) using the finite difference method gives

$$\frac{h_j^{n+1} - h_j^n}{\Delta t} + \frac{1}{\Delta x}\left[F^n_{j+\frac{1}{2}} - F^n_{j-\frac{1}{2}}\right] + \frac{1}{\Delta x}\left[Q^{n+1}_{j+\frac{1}{2}} - Q^{n+1}_{j-\frac{1}{2}}\right] + \frac{1}{\Delta x}\left[R^{n+1}_{j+\frac{1}{2}} - R^{n+1}_{j-\frac{1}{2}}\right] = 0. \tag{23}$$

Note that the flux function, F, in (23) is treated explicitly in time, whereas, Q and R terms are dealt with semi-implicitly to ensure numerical stability as will be shown in the steps below. The values of $F_{j\pm1/2}$ and $Q_{j\pm1/2}$ are computed using the robust (TVD) scheme of Ref. 39 as

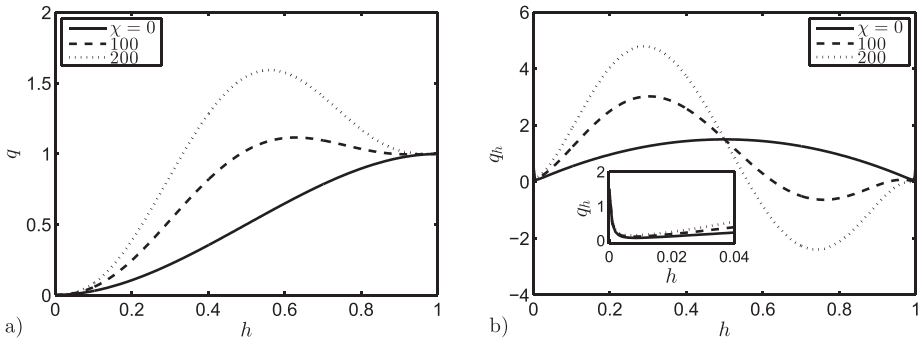

FIG. 2. (a) The dependency of the flux function, q, in (17) on the interface height, h, for $h_x = h_{xxx} = 0$, $m = 1$, and various values of χ. (b) q_h versus h for the same parameters as in (a). The inset shows $q_h \to 1.5$ as $h \to 0$. Similarly, $q_h \to 1.5$ as $h \to 1$.

$$F^n_{j\pm\frac{1}{2}} = \frac{1}{2}\left\{\left[F\left(h^{R,n}_{j\pm\frac{1}{2}}\right)+F\left(h^{L,n}_{j\pm\frac{1}{2}}\right)\right]-a^n_{j\pm\frac{1}{2}}\left[h^{R,n}_{j\pm\frac{1}{2}}-h^{L,n}_{j\pm\frac{1}{2}}\right]\right\}, \tag{24}$$

and

$$Q^{n+1}_{j+\frac{1}{2}} = \frac{1}{2}\left[Q\left(h^n_{j+1},\frac{h^{n+1}_{j+1}-h^{n+1}_j}{\Delta x}\right)+Q\left(h^n_j,\frac{h^{n+1}_{j+1}-h^{n+1}_j}{\Delta x}\right)\right], \tag{25}$$

$$Q^{n+1}_{j-\frac{1}{2}} = \frac{1}{2}\left[Q\left(h^n_j,\frac{h^{n+1}_j-h^{n+1}_{j-1}}{\Delta x}\right)+Q\left(h^n_{j-1},\frac{h^{n+1}_j-h^{n+1}_{j-1}}{\Delta x}\right)\right]. \tag{26}$$

Here,

$$h^{R,n}_{j+\frac{1}{2}} = h^n_{j+1}-\frac{\Delta x}{2}(h^n_x)_{j+1}, h^{L,n}_{j+\frac{1}{2}} = h^n_j+\frac{\Delta x}{2}(h^n_x)_j,$$
$$h^{R,n}_{j-\frac{1}{2}} = h^n_j-\frac{\Delta x}{2}(h^n_x)_j, h^{L,n}_{j-\frac{1}{2}} = h^n_{j-1}+\frac{\Delta x}{2}(h^n_x)_{j-1}, \tag{27}$$

with $(h^n_x)_k$ being a flux limiter chosen to be in the *minmod* class of the following form:

$$(h^n_x)_k = minmod\left(\frac{h^n_k-h^n_{k-1}}{\Delta x},\frac{h^n_{k+1}-h^n_k}{\Delta x}\right). \tag{28}$$

Note that the function *minmod* is defined as

$$minmod\,(a,b) = \frac{1}{2}\left[\mathrm{sgn}\,(a)+\mathrm{sgn}\,(b)\right].\min\left(|a|,|b|\right). \tag{29}$$

Also note that

$$a^n_{j\pm\frac{1}{2}} = \max\left(\left|\frac{\partial F}{\partial h}\right|_{h^{R,n}_{j\pm\frac{1}{2}}},\left|\frac{\partial F}{\partial h}\right|_{h^{L,n}_{j\pm\frac{1}{2}}}\right) \tag{30}$$

gives the local propagation speed of the interfacial wave used to estimate the stable time step, dt, given a Courant–Friedrichs–Lewy (CFL) condition as

$$dt = CFL.dx/\max\left(|a\,(t)|\right). \tag{31}$$

In our case, we have found that $CFL \approx 0.1$ gives stable results. Note that due to the nature of our numerical implementation, the effect of χ (or β) on wave speed (30) is automatically taken care of ensuring the stability of the code. In calculating the $Q^{n+1}_{j\pm1/2}$ terms in (25) and (26), only the derivative terms are expressed implicitly. The fourth order diffusion term, R, in (23) is calculated based on the scheme suggested by Ref. 41 as

$$R^{n+1}_{j+\frac{1}{2}} = R\left(\frac{h^n_{j+1}+h^n_j}{2},\frac{h^{n+1}_{j+2}-3h^{n+1}_{j+1}+3h^{n+1}_j-h^{n+1}_{j-1}}{\Delta x^3}\right), \tag{32}$$

$$R^{n+1}_{j-\frac{1}{2}} = R\left(\frac{h^n_j+h^n_{j-1}}{2},\frac{h^{n+1}_{j+1}-3h^{n+1}_j+3h^{n+1}_{j-1}-h^{n+1}_{j-2}}{\Delta x^3}\right). \tag{33}$$

Again, note that similar to Q terms, only the (third-order) derivative terms in (32) and (33) are expressed implicitly. Therefore, Equation (23) will still be linear for the unknowns h^{n+1}_{j-2}, h^{n+1}_{j-1}, h^{n+1}_j, h^{n+1}_{j+1}, and h^{n+1}_{j+2}. It is not difficult to show that one will finally arrive at the following after using (24)–(26), (32), and (33) in (23):

$$\lambda_1 h^{n+1}_{j-2}+\lambda_2 h^{n+1}_{j-1}+\lambda_3 h^{n+1}_j+\lambda_4 h^{n+1}_{j+1}+\lambda_5 h^{n+1}_{j+2} = h^n_j-\frac{\Delta t}{\Delta x}\left[F^n_{j+\frac{1}{2}}-F^n_{j-\frac{1}{2}}\right], \tag{34}$$

which is a system of linear equations with $\lambda_1,\lambda_2,\ldots,\lambda_5$ being coefficients of all evaluated at time n. Equation (34) can be written in the matrix form as shown below given that all the spatial points j are considered,

$$A^n\vec{h}^{n+1} = \vec{f}^n, \tag{35}$$

where A^n is a pentadiagonal matrix of size $N\times N$ (N being the size of the spatial computational domain), and $\vec{h}^{n+1}$ and $\vec{f}^n$ are vectors of size N. In order to efficiently solve Equation (35), we have used a similar algorithm to that of Thomas which is given in Ref. 42 used in tridiagonal systems based on Gaussian elimination. The numerical examples shown in this paper are attained using the computational resources in the Center for Advanced Computing and Data Systems of the University of Houston (Maxwell cluster). The run time on a single node on such a cluster can take up to a few hours. All the test problems given in Refs. 39 and 40 have been successfully recovered using our numerical formulation.

IV. RESULTS

A. Displacement flow ($\hat{V}_0 > 0$)

Figure 3(a) shows the evolution of the interface height with time assuming two iso-dense, ($\chi = 0$) iso-viscous ($m = 1$) fluids in the miscible limit ($W = 0$). The results are in complete agreement with lubrication model results of Ref. 26. The fluids are initially sharply separated at $x = 0$ over one dx length. As can be seen from the figure, there is a *shock-type* profile formed at the front over long times ($h_f \approx 0.75$). The speed of the front is found to be $V_f \approx 1.125$. Note that a no-slip condition ($\alpha = 0$) has been used in obtaining Fig. 3(a) since shear stress is not singular in the case of miscible fluids.[34] Figure 3(b) depicts the snapshots of experiments carried out similar to our previous work[19] showing the displacement of water ($\hat{\rho}_L = 998.8\,\mathrm{kg/m^3}$) by a slightly heavier salt-water solution ($\hat{\rho}_H = 1019.2\,\mathrm{kg/m^3}$) in an inclined pipe ($\beta = 70°$) with diameter $\hat{D} = 9.53$ mm. Since the theoretical results shown in Fig. 3(a) correspond to a 2D channel geometry, we are not after a one-to-one comparison against the pipe experiments in Fig. 3(b). However, it can be seen that the lubrication model has successfully captured the global effects of the displacement flow in question. For quantitative agreements of miscible lubrication-style models and experiments; see Refs. 23 and 27.

1. *Long-time behavior—Steady traveling wave solution*

The interface profiles shown in Fig. 3(a) suggest a rather *self-similar* pattern in the form of a steady traveling wave. Taghavi *et al.*[26] proved that steady traveling waves cannot exist for the case of *miscible* fluids when using a frame moving with the mean flow speed, i.e., $\eta = x - t$. However, they overlooked the fact that the similarity parameter should also be divided by time ($\eta = (x-t)/t$) as noted in the recent study of Zheng *et al.*[43] Using this similarity parameter and (17), Equation (18) can be re-written as

$$\eta h_\eta - \left[q\left(h,\chi-h_\eta/t+Wh_{\eta\eta\eta}/t^3\right)-h\right]_\eta = 0. \tag{36}$$

Seeking a steady solution at long times ($t\to\infty$) results in

$$\eta h_\eta - \left[q\,(h,\chi)-h\right]_\eta = 0. \tag{37}$$

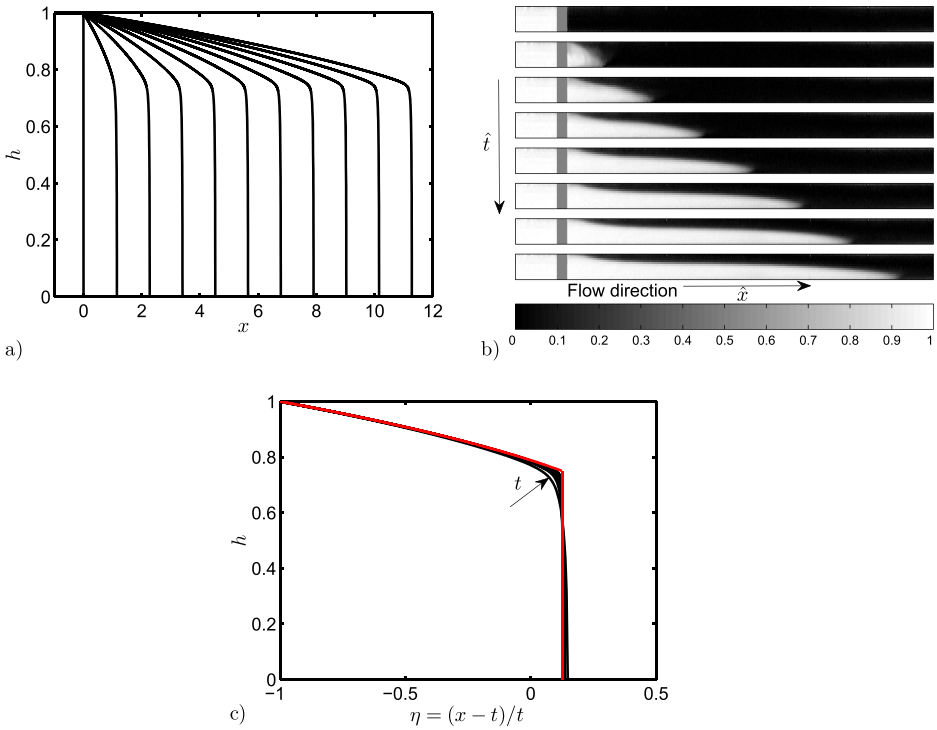

FIG. 3. (a) Evolution of the interface height, h, with time, $t = [0, 1, 2, \ldots, 10]$, in displacement flow of two iso-dense, iso-viscous miscible fluids ($\chi = 0, m = 1, W = 0$). The results are in complete agreement with Ref. 26. (b) Sample snapshots of experiments similar to Ref. 19 obtained for $\chi \approx 84$ ($\beta = 70°$, $Re = 703$, $Fr = 2.4$) and $m = 1$ at times $\hat{t} = [0, 1.72, 3.44, \ldots, 13.75]$ s in circular pipe geometry with diameter 9.53 mm. Length of the domain shown is ≈2 m. The color bar shows the concentration field with 0 and 1 referring to the displaced and displacing fluids, respectively. (c) Collapse of the interface height profiles using a similarity parameter, $\eta = (x - t)/t$. The red line shows the similarity solution obtained from (41).

Alternatively, the following condition can be obtained as follows:

$$\eta - q_h(h, \chi) + 1 = 0, \tag{38}$$

which relates h to η and other parameters of the problem, namely, m and α. For the case shown in Fig. 3 ($\chi = \alpha = W = 0$ and $m = 1$), Equation (38) is reduced to the following simple relation:

$$\eta + 6h^2 - 6h + 1 = 0, \tag{39}$$

which clearly has an analytical expression for h (note that $\eta = -1$ at $h = 1$). However, this solution does not satisfy the total flow rate constraint (13) in the moving frame. Through a novel approach, Zheng *et al.*[43] showed that a compound wave solution may instead be constructed containing a shock front, h_s, located at $\eta_s > 0$ and a stretching region behind ($-1 < \eta < \eta_S$). The shock front location and height are determined from the following condition:

$$\int_{-1}^{\eta_s} h d\eta = 0, \tag{40}$$

as $\eta_s = 1/8$ and $h_s = 3/4$, respectively, which is close to our observation in Fig. 3(a). Therefore, the compound solution is obtained as

$$h = \begin{cases} \left(1 + \sqrt{1 - 2(\eta + 1)/3}\right)/2, & -1 \le \eta \le 1/8 \\ 0, & \eta > 1/8 \end{cases} \tag{41}$$

The compound solution (41) as well as numerically computed interface profiles at long time are shown in Fig. 3(c). Evidently, there is a very close agreement found between the two showing the effectiveness of the similarity solution approach.

Figure 4(a) shows the effect of an interfacial tension on the interface profile evolution suggesting the formation of a *capillary ridge* similar to Refs. 34 and 44 in the middle section of the flow followed by a flat interface height ($h_f \approx 0.8432$, $V_f \approx 1.106$) which is found to grow in length over time. The capillary ridge forming at long times is better depicted in the close-up shown in Fig. 4(b). The immiscible results presented here can potentially vary with the initial condition. However, similar to the miscible limit, we have assumed that the fluids are initially sharply separated at $x = 0$ over one dx length to mimic a neutrally wetting configuration as closely as possible. The dependency of the results on the mesh size is also provided. The results for two different mesh sizes are almost indistinguishable. We have found that $dx = 0.002$ and $CFL = 0.1$ give stable results. Unlike the miscible case, full features of the flow may not be captured for $dx \sim O(10^{-2})$. In comparison with Fig. 3(a), it can be seen that the interfacial tension has slowed down the leading displacement front through increasing the shock height. Taghavi *et al.*[26] found that the overall efficiency of the displacement is proportional to $\sim 1/V_f$, where V_f is the scaled speed of the displacing front. The closer the V_f is to 1, the more efficient the displacement would be. Therefore, for the range given, the immiscibility has enhanced the efficiency of the displacement. Also from Fig. 4, note a slight slip-type effect in the trailing front close to the upper wall, upstream of the capillary ridge region. The collapse of the interface height profiles with the similarity variable $\eta = (x - t)/t$, in the case of immiscible fluids, is investigated in Fig. 4(c). Akin to the miscible case (Fig. 3(c)), the immiscible profiles suggest convergence to a self-similar curve. However, it is not straightforward to obtain an analytical expression in this case as the dynamics is governed by the differential equation (36). The $Wh_{\eta\eta\eta}/t^3$ term in this equation should be treated as $O(1)$ when taking the limit of $t \to \infty$ because of the apparent influence of interfacial tension on long-time interface height profiles (compare Fig. 3(c) and Fig. 4(c)). Another difficulty in finding a similarity solution for immiscible case is the addition of shock-type conditions associated with slippage close to the upper wall.

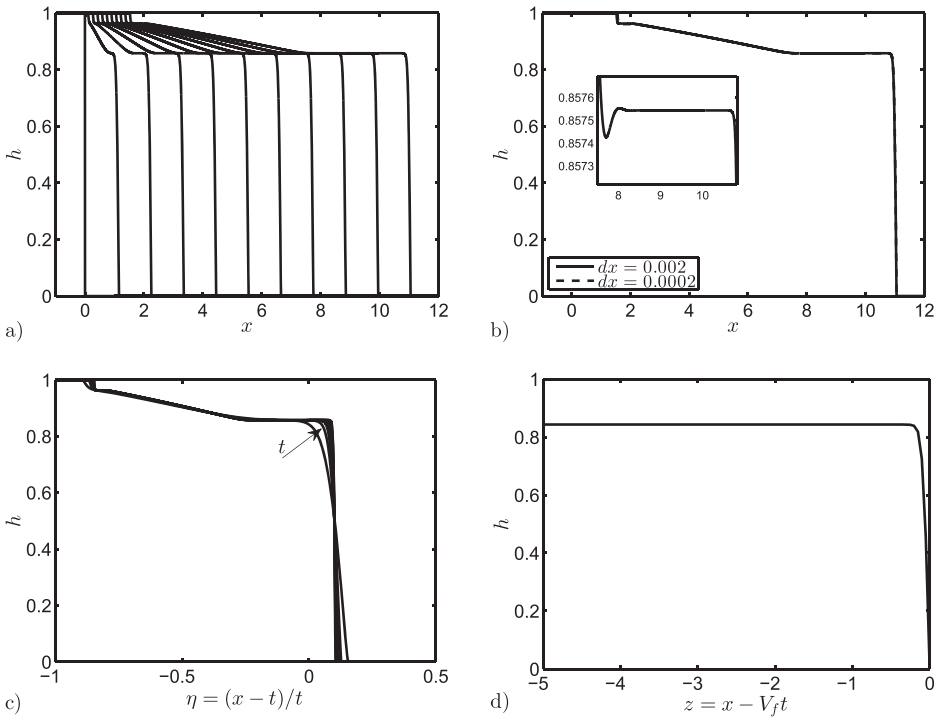

FIG. 4. (a) Evolution of the interface height, h, with time, $t = [0, 1, 2, \ldots, 10]$, in the displacement flow of two iso-dense, iso-viscous immiscible fluids ($\chi = 0$, $m = 1$, $W = 0.01$). (b) Interface height, h, at $t = 10$ obtained from part (a) for two different mesh sizes. The inset depicts the close-up of the displacement front revealing the formation of the capillary ridge. (c) Collapse of the interface height profiles using the similarity parameter, $\eta = (x - t)/t$. (d) Interface height with $z = x - V_f t$ in the vicinity of the frontal region obtained for the same simulation using (44).

2. Frontal region

Having found h_f and V_f in Fig. 4, we may now shift to a frame moving with speed V_f, via defining $z = x - V_f t$. Using (17), the kinematic condition (18) can then be re-written as

$$h_t + \left[q_A + (\chi - h_z + Wh_{zzz})\, q_B - V_f h\right]_z = 0. \tag{42}$$

Seeking a steady solution at long times ($h = h(z)$ only) results in

$$\left[q_A + (\chi - h_z + Wh_{zzz})\, q_B - V_f h\right]_z = 0. \tag{43}$$

Since $q = 0$ at $h = 0$, (43) implies that

$$q_A + (\chi - h_z + Wh_{zzz})\, q_B - V_f h = 0, \tag{44}$$

which is a boundary-value Ordinary Differential Equation (ODE) numerically solvable for $h \in [0, h_f]$ subject to the following conditions:

$$h \to h_f,\ h_z \to 0 \qquad as\ z \to -\infty, \tag{45}$$

$$h \to 0 \qquad as\ z \to 0. \tag{46}$$

The numerical solution of (44) for parameters used in Fig. 4(a) is given in Fig. 4(d). For the given front height and speed values ($h_f = 0.8432$ and $V_f = 1.106$), we can interestingly observe a stable solution which is identical to the frontal region in Fig. 4(a). Such a stable solution cannot be recovered for h_f values other than 0.8432 (results not shown here for brevity).

Figure 5(a) compares the interface profiles at long time ($t = 10$) for $\chi = 0, m = 1$ and different values of the Laplace number. It can be seen that the interfacial tension acts to smoothen out the frontal region of the flow causing a non-monotonic effect on the speed of the front. In fact, it seems that the front is slowed down at small values of W but interestingly is accelerated for higher W due to the profile smoothing effect; see also the inset of Fig. 5(a) showing the disappearance of the capillary ridge at higher W. The effect of χ on the displacement flow of immiscible fluids is shown in Fig. 5(b). The figure suggests that the frontal speed increases as the density difference between the fluids is increased. Note that the increase in frontal speed is achieved through decreasing of the shock height. The effect of a viscosity contrast in the immiscible limit is shown in Fig. 5. It is evident that at lower m values (less viscous displaced fluid), a more efficient displacement has been resulted. We can also interestingly observe there is a higher probability of the trailing front slippage for $m < 1$ in the presence of an interfacial tension. This is due to the fact that for such cases $h \to 1$ close to the upper wall resulting in an increase of the slip velocity; see condition (11). It is useful at this stage to look into streamwise velocity profiles of a typical simulation with viscosity ratio among fluids. Figure 5(d) shows computed velocity profiles using (14) and (15) at different locations, $x = 0, 2.6, 9.7, 11.6, 13.5$, for $m = 2$ case in Fig. 5(c). The profiles are calculated for interface heights, $h = 1, 0.98, 0.789, 0.02, 0$, respectively. It is perceived that there is slippage at the walls when $h = 1$ or 0; see conditions (10) and (11). As soon as there is deviation from these interface heights (e.g., $h = 0.98$ or 0.02), the wall slippage is reduced. Since $m = 2$ corresponds to a less-viscous displacing fluid, we note a larger gradient of velocity within this layer ($h = 0.789$ case in Fig. 5(d)) to ensure homogeneity of the shear stress across the interface; see condition (12).

An important feature in designing the displacement flows is whether there exists a *back flow* of the displaced fluid in the upstream region of the gate valve ($x = 0$) or not. The back flow should be particularly avoided in operations related to the primary cementing of oil and gas wells.[1] In the miscible limit, the back flow is dictated by the critical parameter $\chi_c \approx 69.94$.[18] When $\chi > \chi_c$ there will always form a back flow. Figure 6(a) shows that in the presence of (a fairly small) interfacial tension, the critical χ_c does seem to still be the defining back flow criterion. As can be noted from the figure, the trailing edge does travel upstream of the gate region ($x < 0$) for $\chi > \chi_c$.

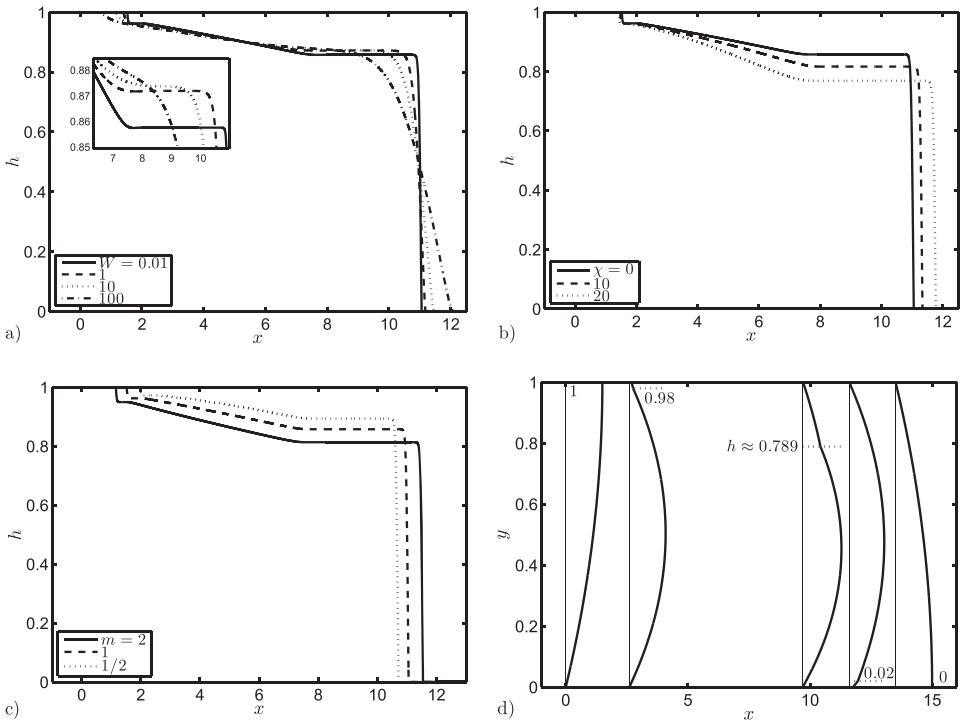

FIG. 5. Comparison of the interface height, h, at $t = 10$ for (a) $\chi = 0$, $m = 1$ at different values of W, (b) $W = 0.01$, $m = 1$ at different values of χ, and (c) $\chi = 0$, $W = 0.01$ at different values of m. The inset in part (a) shows the close-up of the displacement front. (d) Velocity profile plotted at locations $x = 0$, 2.6, 9.7, 11.6, and 13.5 corresponding to different dotted interface heights, $h = 1$, 0.98, 0.789, 0.02, and 0, for $m = 2$ case in part (c).

As the close-up in the figure suggests, the trailing front interface height just before the back flow ($\chi < \chi_c$) is more than that of the leading front. However, after the critical point is passed, the trailing front height interestingly drops below the leading front height. Upon progressively increasing the density difference through χ parameter beyond the critical value, χ_c, one expects the formation of a stronger back flow. Figure 6(b) shows the long time interface height profiles for $\chi = 150$ and $W = 0, 0.01$. There is a noteworthy modification of the (leading and trailing) frontal height and speed upon the formation of two capillary ridges in the flow. In simple words, it seems as though the surface tension (at least for small W) is acting to hold the flow together by hindering the counter-current of the layers.

B. Exchange flow ($\hat{V}_0 = 0$)

The total flow rate constraint (13) implies a *displacement* configuration where there exists a net flow from the displacing side to the displaced one ($\hat{V}_0 > 0$). In the absence of a mean flow ($\hat{V}_0 = 0$), one recovers an *exchange* flow, i.e., the flow driven purely by buoyancy.[25] The following total flow rate constraint shall then be used instead:

$$\int_0^1 u dy = 0. \tag{47}$$

The flux function, q, in the form of (17) can consequently be calculated giving q_A and q_B. It is not difficult to show that in the case of exchange flow, the advective flux, q_A, is zero, while the buoyancy-driven flux, q_B, remains intact. In other words,

$$q_A = 0, \tag{48}$$

$$q_B = q_B. \tag{49}$$

The kinematic condition (19) may be solved using the same numerical scheme explained in Section III. Note that the flow behavior in the model is still captured via the χ parameter which is immaterial of $\hat{V}_0$. Therefore, $\hat{V}_0 = 0$ will not impose any singularity in the exchange flow model.

Figures 7(a) and 7(b) show the interface height profiles, h, for exchange flows at time $t = 10$ and different values of W obtained for $\chi = 10$ and 30, respectively. First thing to notice upon comparison with displacement results (Fig. 4, for instance) is that the flow in the case of exchange is *symmetric* with respect to x, which is also reported in Refs. 14 and 30.

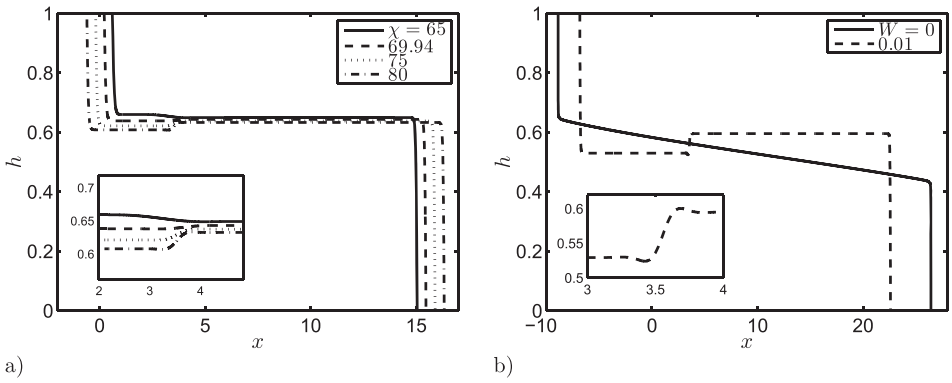

FIG. 6. (a) Change in the interface height profile, h, for $m = 1$ and $W = 0.01$ at $t = 10$ in the vicinity of the critical $\chi_c \approx 69.94$. (b) Interface height, h, plotted at $t = 10$ for $m = 1$, $\chi = 150$, and $W = 0, 0.01$. The inset shows the close-up of the intermediate capillary ridge region causing jump in the interface height.

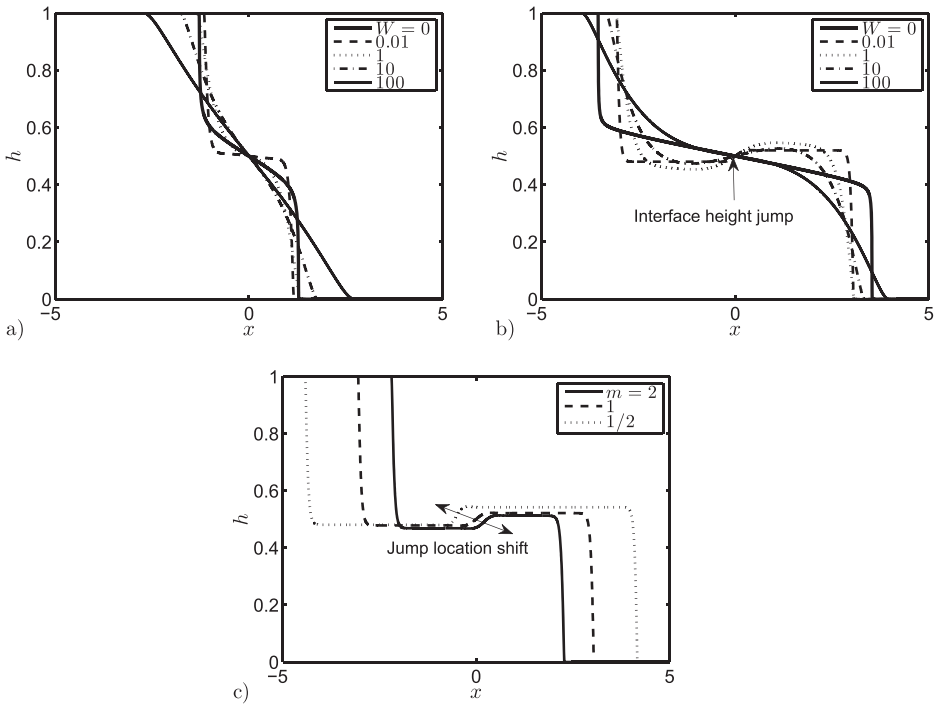

FIG. 7. Change in the interface height profile, h, of exchange flow for $m = 1$, $t = 10$, and various values of W obtained for (a) $\chi = 10$ and (b) $\chi = 30$. (c) Interface height profile obtained for $\chi = 30$, $W = 0.01$, $t = 10$, and various values of viscosity ratio, m, indicating a shift in the location of the interface jump point.

Note the slower flow advancement for $\chi = 10$ case (Fig. 7(a)) compared to $\chi = 30$ (Fig. 7(b)). The driving buoyancy force in the former is less than that of latter. The pattern observed in Fig. 5(a) with W for the displacement flow case approximately holds also in the exchange flow. It is observed that small values of surface tension parameter yield to a capillary ridge decelerating the heavy and light layers compared to the miscible case ($W = 0$). However, as W is increased, a smoothing effect is observed. Interestingly, at a higher value of χ (Fig. 7) and for rather small values of W, there is a jump observed in the interface height close to the gate region ($x = 0$). The heavy layer has a higher h value than the light one. Similar jumping behavior has been observed in lattice Boltzmann simulations of Refs. 30 and 31 for viscous flows carried in the 2D channel geometry. The effect of a viscosity ratio between two fluids on the interface height is investigated in Fig. 7(c). The spreading of the interface appears to be maximal/minimal for low/high values of m. This observation is in line with findings of Refs. 26 and 33 for miscible fluids. Similar jump-type behavior across the interface to the iso-viscous case (Fig. 7(b)) is moreover observed. However, there appears to be a shift in the location of the jump point with m. This is possibly due to the fact that in the presence of a viscosity ratio between the two fluids, the flow becomes asymmetric, even for miscible case, on the right and left hand sides. Surface tension will then act to intensify such flow asymmetry resulting to a shift in the location of the jump point.

1. Short-time behavior

The early stage of a displacement flow in a frame moving with speed 1 is, in fact, similar to that of an exchange configuration where gravitational spreading (proportional to the slope of the interface) dominates the imposed flow.[26] In this case, a similarity parameter, $\zeta = x/\sqrt{t}$, can capture the dynamics of the flow over short time; see Refs. 26 and 33. Using this similarity parameter and (17), (48), and (49), Equation (18) can then be re-written as

$$\frac{1}{2}\zeta h_\zeta + \left[q_B h_\zeta\right]_\zeta - \sqrt{t}\left[\chi q_B\right]_\zeta - \frac{1}{t}\left[W q_B h_{\zeta\zeta\zeta}\right]_\zeta = 0. \quad (50)$$

In the absence of an interfacial tension ($W = 0$) and considering short times ($t \to 0$), one would obtain the following equation governing the interface height similarity solution:

$$\frac{1}{2}\zeta h_\zeta + \left[q_B h_\zeta\right]_\zeta = 0. \quad (51)$$

Based on the numerical solution shown, e.g., in Fig. 7(a) for miscible fluids ($W = 0$), it can be seen that close to the walls ($h \to 0, 1$) the slope of h becomes singular, i.e., $h_\zeta \to -\infty$; see also Ref. 32. Therefore, it is more convenient to work with $\zeta(h)$ instead of $h(\zeta)$. It is not difficult to re-write Equation (51) as

$$\zeta_{hh} - \frac{1}{q_B}\left(\frac{1}{2}\zeta(\zeta_h)^2 + q_{B,h}\zeta_h\right) = 0. \quad (52)$$

Equation (52) may be solved numerically subject to the boundary conditions $\zeta_h(h = 0) = \zeta_h(h = 1) = 0$. However, it is more convenient to solve (52) via a shooting method.[26,32,43] For the case of iso-viscous fluids, one would expect symmetry, i.e., $\zeta(h = 0.5) = 0$. Choosing an arbitrary slope value for $\zeta_h(h = 0.5)$ one may solve (52) over, for example, $h \in [0.5, 1]$ until boundary condition $\zeta_h(h = 1) = 0$ is satisfied. This solution, which is similar to that of Taghavi *et al.*,[26] is plotted in Fig. 8 showing an excellent agreement with the numerical solution of the lubrication model Partial Differential Equation (PDE) (18) at short time ($t = 0.001$).

In the case of immiscible fluids ($W \neq 0$), Equation (50), however, suggests that the interfacial tension term, $\left[W q_B h_{\zeta\zeta\zeta}\right]_\zeta$, dominates other terms since $1/t \to \infty$ as $t \to 0$. The solution of this governing equation is in the following form:

$$q_B h_{\zeta\zeta\zeta} = c, \quad (53)$$

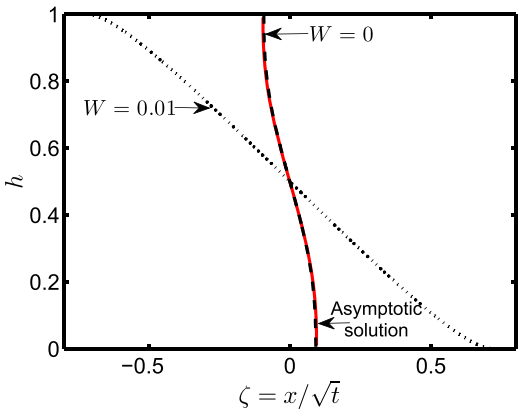

FIG. 8. Short-time behavior of the interface height, h, plotted at $t = 0.001$ versus $\zeta = x/\sqrt{t}$ for $m = 1$, $\chi = 10$, and $W = 0$ and 0.01. The solid red line indicates asymptotic solution (52) for the miscible case ($W = 0$).

where c is a constant. Alternatively,

$$\zeta_{hhh} - 3(\zeta_h)^{-1}(\zeta_{hh})^2 + \frac{c}{q_B}(\zeta_h)^4 = 0. \tag{54}$$

Numerical solution of (54) via a shooting method is more involved than (52) due to the additional boundary conditions required. However, a short time solution of the full lubrication model PDE (18) in the presence of an interfacial tension ($W = 0.01$) is added to Fig. 8 for comparison with the miscible case. The spreading of the interface over a larger domain of ζ is evident which is in line with the suggestion of asymptotic analysis (50). In other words, it may be concluded that the dynamics of the interface at short times is dominated by the interfacial tension as opposed to buoyancy. As time is increased, the slope of the interface changes too altering the overall dynamics of the flow. Upon comparing Figs. 7(a) and 8, it can be observed that even though the interface height for the immiscible case is more diffuse at the beginning of the experiment, over long times, the heavy and light fronts can spread further in the miscible case.

V. CONCLUSIONS AND FUTURE WORKS

Displacement flow of two immiscible Newtonian fluids in an inclined duct (two-dimensional channel) has been investigated theoretically via developing a lubrication model. The displacing fluid is denser than the displaced fluid (i.e., unstable density) both behaving as neutrally wetting in contact with the solid boundary. In comparison with the miscible fluids limit studied well in the literature, it is found that the fluids immiscibility causes a *capillary ridge* in the vicinity of the displacing front, which diminishes as the surface tension is increased. There is a novel slip-type behavior also present in the vicinity of the top wall in the immiscible case. For small values of the Laplace number (surface tension parameter), the fluids immiscibility is found to decelerate the advancement of interpenetrating heavy and light layers. The frontal region of the flow is calculated semi-analytically by switching to a moving frame of reference showing agreement with numerical results. The displacement front velocity is decreased (resulting to a higher efficiency) when density difference is small and/or the displacing fluid is more viscous. While a similarity solution is easily attainable for the miscible case, the analysis for the immiscible limit is more involved. The limit of zero imposed velocity corresponding to the *exchange* flow has further been investigated. Similar capillary-ridge patterns have been identified within the heavy and light fingers. In addition, there forms an interesting jump in the interface close to the vicinity of the gate valve region, which is also reported in recent lattice Boltzmann simulations of Ref. 30. Through an asymptotic analysis approach, it is found that the dynamics of flow at early stages of the release is dominated by diffusive interfacial tension effects. A final note here is that the experimental investigation of the neutrally wetting problem in hand is slightly challenging since various immiscible oil/water systems exhibit partial non-wetting/wetting adjacent to the solid duct walls such as the study of Ref. 29. However, if the inner region of the duct is covered with appropriate coatings there can be a possibility of obtaining neutrally wetting setting for both fluids present comparing against the theoretical predictions of the developed model.

ACKNOWLEDGMENTS

This research has been carried out at the University of Houston (UH). We thank the Center for Advanced Computing and Data Systems (CACDS) in UH for providing us with their great computational resources and assistance. The authors highly appreciate useful discussion with Dr. N. Singh from UH regarding the execution of computational codes. Moreover, A. Hasnain acknowledges the support received from Houston Scholars Program during summer 2016. Constructive comments from the reviewers in improving the manuscript are highly appreciated as well.

APPENDIX A: COEFFICIENTS IN VELOCITY EXPRESSIONS (14) AND (15)

$$\begin{aligned} p_{0,x} = {} & (-6\alpha h^4 m^2 - 3h^6 m + 6\alpha h^4 m + 18\alpha h^3 m^2 + 3h^6 + 21h^5 m + 4\alpha^2 h m^2 - 14\alpha h^3 m \\ & - 12\alpha h^2 m^2 - 15h^5 - 45h^4 m - 4\alpha^2 m^2 + 6\alpha h^2 m + 30h^4 + 39h^3 m + 6\alpha h m - 30h^3 - 12h^2 m - 4\alpha m \\ & + 15h^2 - 3h)(\chi - h_x + W h_{xxx})/L + (36h^3 m^2 - 36h^3 m - 36h^2 m^2 - 12\alpha m^2 + 72h^2 m - 36h m)/L, \end{aligned} \tag{A1}$$

$$\begin{aligned} c_1 = {} & h(4\alpha h^4 m^2 + 3h^6 m - 4\alpha h^4 m - 10\alpha h^3 m^2 - 3h^6 - 15h^5 m + 12\alpha h^3 m + 6\alpha h^2 m^2 \\ & + 15h^5 + 27h^4 m - 12\alpha h^2 m - 30h^4 - 21h^3 m + 4\alpha h m + 30h^3 + 6h^2 m - 15h^2 + 3h)(\chi - h_x + W h_{xxx})/L \\ & + h(-18h^3 m^2 + 18h^3 m + 18h^2 m^2 + 12\alpha m^2 - 18h^2 m - 18h m + 18m)/L, \end{aligned} \tag{A2}$$

$$c_2 = \alpha c_1/(3h), \tag{A3}$$

$$\begin{aligned} d_1 = &-h(-3h^6m - 4\alpha h^4m + 3h^6 + 3h^5m + 4\alpha h^4 + 2\alpha h^3m - 3h^5 - 4\alpha h^3 \\ &+ 6\alpha h^2m + 3h^4 + 4\alpha^2m - 9h^3 - 4\alpha h + 6h^2 + 4\alpha)(\chi - h_x + Wh_{xxx})/L \\ &- h(18h^3m - 18h^3 - 18h^2m - 12\alpha m + 18h^2 + 18h - 18)/L, \end{aligned} \tag{A4}$$

$$\begin{aligned} d_2 = &(1/6)(6\alpha h^6m^2 + 8\alpha^2h^4m^2 - 6\alpha h^6m - 6\alpha h^5m^2 - 18h^7m - 8\alpha^2h^4m - 8\alpha^2h^3m^2 - 18\alpha h^5m + 18h^7 \\ &+ 27h^6m + 12\alpha^2h^3m + 24\alpha h^5 + 36\alpha h^4m - 27h^6 - 9h^5m - 42\alpha h^4 + 9h^5 + 8\alpha^2hm + 18\alpha h^3 - 9h^4 \\ &- 6\alpha h^2 + 9h^3 + 6\alpha h)(\chi - h_x + Wh_{xxx})/L + (1/6)(-36\alpha h^3m^2 + 36\alpha h^3m + 72\alpha h^2m^2 + 108h^4m + 24\alpha^2m^2 \\ &- 72\alpha h^2m - 108h^4 - 216h^3m - 36\alpha hm + 216h^3 + 108h^2m + 36\alpha m - 108h^2)/L. \end{aligned} \tag{A5}$$

Here,

$$\begin{aligned} L = &-3h^6m^2 + 6h^6m + 3h^5m^2 - 8\alpha h^3m^2 - 3h^6 - 18h^5m + 8\alpha h^3m + 12\alpha h^2m^2 + 15h^5 + 30h^4m \\ &+ 4\alpha^2m^2 - 12\alpha h^2m - 30h^4 - 30h^3m + 30h^3 + 12h^2m + 4\alpha m - 15h^2 + 3h. \end{aligned} \tag{A6}$$

APPENDIX B: FLUX FUNCTIONS q_A AND q_B IN (17)

$$\begin{aligned} q_A = &\, hm(-3h^5m - 6\alpha h^3m + 3h^5 + 3h^4m + 6\alpha h^3 + 10\alpha h^2m + 3h^4 + 4\alpha^2m - 6\alpha h^2 - 15h^3 - 6\alpha h + 9h^2 + 6\alpha)/ \\ &(-3h^6m^2 + 6h^6m + 3h^5m^2 - 8\alpha h^3m^2 - 3h^6 - 18h^5m + 8\alpha h^3m + 12\alpha h^2m^2 + 15h^5 + 30h^4m + 4\alpha^2m^2 \\ &- 12\alpha h^2m - 30h^4 - 30h^3m + 30h^3 + 12h^2m + 4\alpha m - 15h^2 + 3h), \end{aligned} \tag{B1}$$

$$\begin{aligned} q_B = &\frac{h^2(h-1)^2}{3}(3\alpha h^3m^2 + 3h^5m + 4\alpha^2hm^2 - 3h^5 - 6h^4m - 4\alpha^2hm - 3\alpha h^3 - 4\alpha h^2m + 9h^4 \\ &+ 3h^3m + 4\alpha^2m + 9\alpha h^2 + 4\alpha hm - 9h^3 - 9\alpha h + 3h^2 + 3\alpha)/ \\ &(-3h^6m^2 + 6h^6m + 3h^5m^2 - 8\alpha h^3m^2 - 3h^6 - 18h^5m + 8\alpha h^3m + 12\alpha h^2m^2 + 15h^5 + 30h^4m + 4\alpha^2m^2 \\ &- 12\alpha h^2m - 30h^4 - 30h^3m + 30h^3 + 12h^2m + 4\alpha m - 15h^2 + 3h). \end{aligned} \tag{B2}$$

Setting $\alpha = 0$ in the above, the flux expressions of Ref. 26 for miscible fluids will be recovered as

$$q_A = \frac{3mh^2(mh^2 + (h+3)(1-h))}{3[(1-h)^4 + 2mh(1-h)(h^2 - h + 2) + m^2h^4]} \tag{B3}$$

and

$$q_B = \frac{h^3(1-h)^3(mh + (1-h))}{3[(1-h)^4 + 2mh(1-h)(h^2 - h + 2) + m^2h^4)]}. \tag{B4}$$

[1] E. Nelson and D. Guillot, *Well Cementing*, 2nd ed. (Schlumberger Educational Services, 2006).
[2] K. Ruschak, "Coating flows," Annu. Rev. Fluid Mech. **17**(1), 65–89 (1985).
[3] R. Valette, P. Laure, Y. Demay, and J. Agassant, "Convective linear stability analysis of two-layer coextrusion flow for molten polymers," J. Non-Newtonian Fluid Mech. **121**(1), 41–53 (2004).
[4] M. Parvez, N. Ong, Y. Lam, and S. Tor, "Gas-assisted injection molding: The effects of process variables and gas channel geometry," J. Mater. Process. Technol. **121**(1), 27–35 (2002).
[5] P. Howell, S. Waters, and J. Grotberg, "The propagation of a liquid bolus along a liquid-lined flexible tube," J. Fluid Mech. **406**, 309–335 (2000).
[6] O. Wanner, H. Eberl, E. Morgenroth, D. Noguera, C. Picioreanu, B. Rittmann, and M. Van Loosdrecht, *Mathematical Modeling of Biofilms*, Scientific and Technical Report Series (IWA, 2006), Vol. 18, pp. 1–199.
[7] D. Burfoot, K. Middleton, and J. Holah, "Removal of biofilms and stubborn soil by pressure washing," Trends Food Sci. Technol. **20**, S45–S47 (2009).
[8] G. Christian and P. Fryer, "The effect of pulsing cleaning chemicals on the cleaning of whey protein deposits," Food Bioprod. Process. **84**, 320–328 (2006).
[9] P. Fryer, G. Christian, and W. Liu, "How hygiene happens: Physics and chemistry of cleaning," Int. J. Dairy Technol. **59**(2), 76–84 (2006).
[10] M. Regner, M. Henningsson, J. Wiklund, K. Östergren, and C. Trägårdh, "Predicting the displacement of yoghurt by water in a pipe using CFD," Chem. Eng. Technol. **30**(7), 844–853 (2007).
[11] P. Cole, K. Asteriadou, P. Robbins, E. Owen, G. Montague, and P. Fryer, "Comparison of cleaning of toothpaste from surfaces and pilot scale pipework," Food Bioprod. Process. **88**(4), 392–400 (2010).
[12] B. Al Khayyat, J. A. Morris, K. Ravi, and J. Faria, "Successes in production-liner cementing in oil-based mud: A case study," in *SPE/IADC Middle East Drilling Technology Symposium* (Society of Petroleum Engineers, 1999), pp. 193–204.
[13] T. Seon, J.-P. Hulin, D. Salin, B. Perrin, and E. Hinch, "Buoyant mixing of miscible fluids in tilted tubes," Phys. Fluids **16**, L103–L106 (2004).
[14] T. Seon, J.-P. Hulin, D. Salin, B. Perrin, and E. Hinch, "Buoyancy driven miscible front dynamics in tilted tubes," Phys. Fluids **17**, 031702 (2005).
[15] T. Seon, J.-P. Hulin, D. Salin, B. Perrin, and E. Hinch, "Laser-induced fluorescence measurements of buoyancy driven mixing in tilted tubes," Phys. Fluids **18**, 041701 (2006).
[16] T. Seon, J. Znaien, D. Salin, J.-P. Hulin, E. Hinch, and B. Perrin, "Front dynamics and macroscopic diffusion in buoyant mixing in a tilted tube," Phys. Fluids **19**, 125105 (2007).
[17] S. Taghavi, T. Seon, D. Martinez, and I. Frigaard, "Influence of an imposed flow on the stability of a gravity current in a near horizontal duct," Phys. Fluids **22**, 031702 (2010).
[18] S. Taghavi, T. Seon, K. Wielage-Burchard, D. Martinez, and I. Frigaard, "Stationary residual layers in buoyant Newtonian displacement flows," Phys. Fluids **23**, 044105 (2011).
[19] K. Alba, S. Taghavi, and I. Frigaard, "Miscible density-unstable displacement flows in inclined tube," Phys. Fluids **25**, 067101 (2013).
[20] K. Alba, S. Taghavi, J. de Bruyn, and I. Frigaard, "Incomplete fluid–fluid displacement of yield-stress fluids. Part 2: Highly inclined pipes," J. Non-Newtonian Fluid Mech. **201**, 80–93 (2013).

[21] S. Taghavi, K. Alba, and I. Frigaard, "Buoyant miscible displacement flows at moderate viscosity ratios and low Atwood numbers in near-horizontal ducts," Chem. Eng. Sci. **69**, 404–418 (2012).
[22] S. Taghavi, K. Alba, M. Moyers-Gonzalez, and I. Frigaard, "Incomplete fluid-fluid displacement of yield stress fluids in near-horizontal pipes: Experiments and theory," J. Non-Newtonian Fluid Mech. **167-168**, 59–74 (2012).
[23] S. Taghavi, K. Alba, T. Seon, K. Wielage-Burchard, D. Martinez, and I. Frigaard, "Miscible displacement flows in near-horizontal ducts at low Atwood number," J. Fluid Mech. **696**, 175–214 (2012).
[24] K. Alba, S. Taghavi, and I. Frigaard, "Miscible heavy-light displacement flows in an inclined two-dimensional channel: A numerical approach," Phys. Fluids **26**(12), 122104 (2014).
[25] T. Seon, J. Znaien, D. Salin, J.-P. Hulin, E. Hinch, and B. Perrin, "Transient buoyancy-driven front dynamics in nearly horizontal tubes," Phys. Fluids **19**, 123603 (2007).
[26] S. Taghavi, T. Seon, D. Martinez, and I. Frigaard, "Buoyancy-dominated displacement flows in near-horizontal channels: The viscous limit," J. Fluid Mech. **639**, 1–35 (2009).
[27] M. Moyers-Gonzalez, K. Alba, S. Taghavi, and I. Frigaard, "A semi-analytical closure approximation for pipe flows of two Herschel-Bulkley fluids with a stratified interface," J. Non-Newtonian Fluid Mech. **193**, 49–67 (2013).
[28] K. Alba, S. Taghavi, and I. Frigaard, "A weighted residual method for two-layer non-Newtonian channel flows: Steady-state results and their stability," J. Fluid Mech. **731**, 509–544 (2013).
[29] J. Hulin, J. Znaien, L. Mendonca, A. Sourbier, F. Moisy, D. Salin, and E. Hinch, "Buoyancy driven interpenetration of immiscible fluids of different densities in a tilted tube," in *APS Division of Fluid Dynamics* (American Physical Society, 2008), Vol. 1.
[30] K. Sahu and S. Vanka, "A multiphase lattice Boltzmann study of buoyancy-induced mixing in a tilted channel," Comput. Fluids **50**(1), 199–215 (2011).
[31] P. Redapangu, S. Vanka, and K. Sahu, "Multiphase lattice Boltzmann simulations of buoyancy-induced flow of two immiscible fluids with different viscosities," Eur. J. Mech.-B Fluids **34**, 105–114 (2012).
[32] J. Martin, N. Rakotomalala, L. Talon, and D. Salin, "Viscous lock-exchange in rectangular channels," J. Fluid Mech. **673**, 132–146 (2011).
[33] G. Matson and A. Hogg, "Viscous exchange flows," Phys. Fluids **24**(2), 023102 (2012).
[34] M. Spaid and G. Homsy, "Stability of Newtonian and viscoelastic dynamic contact lines," Phys. Fluids **8**(2), 460–478 (1996).
[35] V. Ajaev, "Coating flows and contact line models," in *Interfacial Fluid Mechanics* (Springer, 2012), pp. 39–69.
[36] H. Greenspan, "On the motion of a small viscous droplet that wets a surface," J. Fluid Mech. **84**(01), 125–143 (1978).
[37] A. Mazouchi, C. Gramlich, and G. Homsy, "Time-dependent free surface Stokes flow with a moving contact line. I. Flow over plane surfaces," Phys. Fluids **16**(5), 1647–1659 (2004).
[38] K. Yokoi, D. Vadillo, J. Hinch, and I. Hutchings, "Numerical studies of the influence of the dynamic contact angle on a droplet impacting on a dry surface," Phys. Fluids **21**(7), 072102 (2009).
[39] A. Kurganov and E. Tadmor, "New high-resolution central schemes for nonlinear conservation laws and convection–diffusion equations," J. Comput. Phys. **160**(1), 241–282 (2000).
[40] E. Momoniat, C. Harley, and E. Adlem, "Numerical investigation of the generalized lubrication equation," Appl. Math. Comput. **217**(6), 2631–2638 (2010).
[41] Y. Ha, Y. Kim, and T. Myers, "On the numerical solution of a driven thin film equation," J. Comput. Phys. **227**(15), 7246–7263 (2008).
[42] D. Von Rosenberg, "Methods for the numerical solution of partial differential equations," Mod. Analytic Comput. Methods Sci. Math. **16**, 140 (1969).
[43] Z. Zheng, L. Rongy, and H. Stone, "Viscous fluid injection into a confined channel," Phys. Fluids **27**(6), 062105 (2015).
[44] M. Eres, L. Schwartz, and R. Roy, "Fingering phenomena for driven coating films," Phys. Fluids **12**(6), 1278–1295 (2000).